PROCEEDINGS OF THE ROYAL SOCIETY A

rspa.royalsocietypublishing.org

Research

Article submitted to journal

Subject Areas:
mechanical engineering, mathematical modelling

Keywords:
abrasive waterjet, stochastic modelling, machining, erosion

Author for correspondence:
J. Billingham
e-mail: John.Billingham@nottingham.ac.uk

Stochastic Simplified Modelling of Abrasive Waterjet Footprints

P. Lozano Torrubia[1], J. Billingham[2] and D.A. Axinte[1]

[1] Faculty of Engineering, Department of Mechanical Materials and Manufacturing Engineering, University of Nottingham, Nottingham NG7 2RD, UK
[2]School of Mathematical Sciences, University of Nottingham, Nottingham NG7 2RD, UK

Abrasive micro-waterjet processing is a non-conventional machining method that can be used to manufacture complex shapes in difficult-to-cut materials. Predicting the effect of the jet on the surface for a given set of machine parameters is a key element of controlling the process. However, the noise of the process is significant, making it difficult to design reliable jet-path strategies that produce good quality parts via controlled-depth milling. The process is highly unstable and has a strong random component that can affect the quality of the workpiece, especially in the case of controlled-depth milling. This study describes a method to predict the variability of the jet footprint for different jet feed speeds. A stochastic partial differential equation is used to describe the etched surface as the jet is moved over it, assuming that the erosion process can be divided into two main components: a deterministic part that corresponds to the average erosion of the jet, and a stochastic part that accounts for the noise generated at different stages of the process. The model predicts the variability of the trench profiles to within $< 8\%$. These advances could enable abrasive micro-waterjet technology as a suitable technology for controlled-depth milling.

Royal Society Publishing
Informing the science of the future

1. Introduction

Abrasive Waterjet (AWJ) machining is a non-traditional machining process that is being developed in order to manufacture complex 3D parts with difficult to machine materials. Like other non-conventional machining methods, AWJ machining, is a tool-free (i.e. utilises a jet plume instead of a contact tool) technique that is cost efficient [1], but also has other important advantages such as low cutting forces [2], a non existent heat affected zone, and the ability to erode almost any material, independent of its properties [3,4].

The AWJ process consists of a high speed water jet that accelerates abrasive particles to velocities of up to $750m/s$ [5], depending on the pressure of the pump. The mixture of high-speed water and abrasive garnet particles is focused by a nozzle, and this produces a circular high-energy jet that can erode the target material. The erosion rate of the process and the shape that the jet leaves on the target during AWJ controlled-depth milling can be manipulated by varying several parameters, such as the mass flow rate of the abrasive particles, $\dot{m}_a$, the pressure of the pump, P, and the feed speed at which the jet is moved, v_f. In order to produce a given 3D shape, it is therefore necessary to understand the effect of these parameters to determine how to move the jet. The limitations imposed by other factors, such as the jet size, which constrains the size of features that can be machined, must also be considered. An example of the problem is given in figure 1, showing how a single straight jet pass generates a trench. A single straight jet pass is regarded as the most basic entity that can be studied, since it is difficult to obtain an isolated footprint.

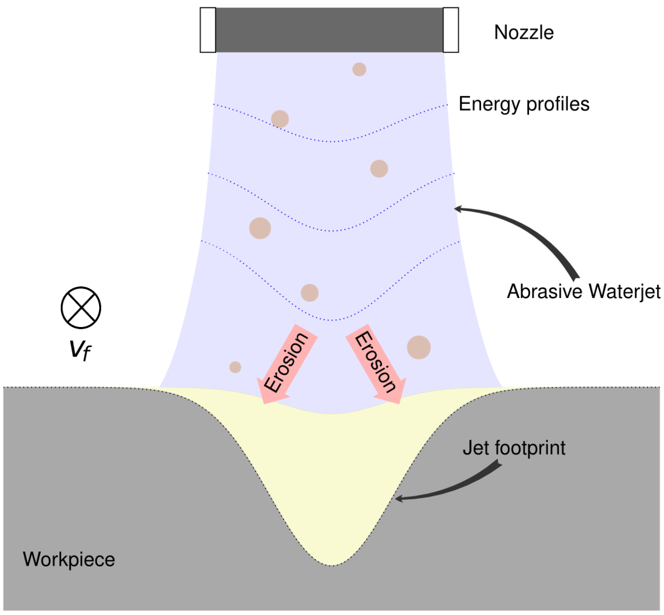

Figure 1: Sketch of the generation of an abrasive waterjet milled channel. The trench is formed by the jet as it moves over the workpiece.

The problem of predicting the depth of penetration or, more importantly, the shape of the jet footprint, has led to extensive research on predictive models for different abrasive jet processes.

A common approach is to use finite element models of multiple particles hitting the surface at high velocity [6–8]. These simulations are computationally expensive, which makes the models difficult to use when investigating how to machine parts with large features. Significant effort has also been put into the development of simplified surface evolution models based on partial differential equations to predict the effect of the jet on the workpiece, from early work [9], which is an attempt to estimate the effect of powder blasting on glass, to more advanced methodologies presented in [10,11]. The main advantage of this methodology is the ability to predict the jet footprint without using complex models, leading to more flexible frameworks that can potentially be used by the machine operator in real time. One of these alternatives is based on an evolution equation whose parameters can be estimated from a small amount of experimental data [11–13]. The challenge addressed by these methods is to relate the operating parameters, particularly the feed speed of the jet, to the average profile of the jet footprint. However, AWJ milling is a highly fluctuating process, since several parts of the system undergo significant variations during the process. The pressure in the pump is constantly fluctuating, since it has an inherent pulsating nature, and this fluctuation affects the water, which influences the mass flow rate and the velocities of the abrasive particles when they are entrained into the jet stream. Moreover, the entrainment process of these particles into the water leads to instabilities that are ultimately reflected on the AWJ milled surface. These variations in the surface can be visualized in the example shown in figure 2, in contrast with the diagram of figure 1 where a smooth idealized trench is presented.

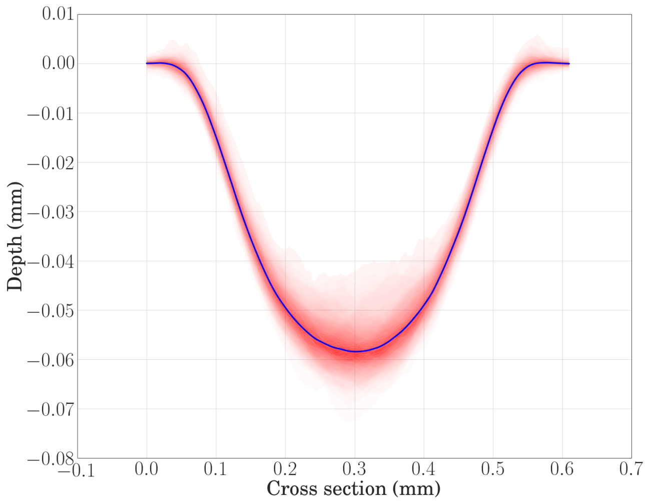

Figure 2: Cross section of an AWJ milled trench, showing a distribution of profiles around an average footprint. The trench was machined at P $= 138MPa$, $v_f = 41.67mm/s$, $\dot{m}_a = 0.5g/s$, a nozzle of diameter $0.5mm$ and garnet abrasive particles of mesh size #220.

The high variability observed in the etched surfaces means that average jet footprint predictions, as developed in previous research, cannot provide enough information about the system to understand the variabilities of 3D milled surfaces. Such variability has given rise to several modelling frameworks that have included stochastic methods to account for such fluctuations. An early method consisted of a unit-event based model [14], overlapping several damage events that account for impacts with different particle size, velocity and position using a probabilistic input. A later model used a similar unit-event framework by adding multiple single particle impacts [15]. More advanced simulation frameworks were introduced for AWJ cutting to predict the quality of the cut [16,17]; the process variability is even more important for controlled-depth milling, since the fluctuations are directly transferred to the surface. This issue has also been addressed using finite element analysis [7,8,18,19], but these methods are computationally expensive and cannot be implemented into optimisation routines for designing jet-path strategies. None of these alternatives has attempted to estimate the inherent noise of the jet in order to take it into account in the surface evolution model. An alternative solution is proposed in [20], but the method requires the periodic performance of calibration channels to account for the fluctuations in the erosion rate. It is necessary to develop a system that runs independently after an initial calibration procedure that requires a minimum set of experimental tests.

In this paper, a novel approach to predict the variability of the jet footprint at different jet feed speeds has been investigated. Furthermore, the proposed methodology aims at providing a procedure to estimate the parameters of the model using a reduced amount of experimental data. The use of stochastic partial differential equations provides a very flexible framework to model the fluctuations of surfaces etched using abrasive waterjet controlled-depth milling. The model can be solved numerically using Monte Carlo methods, but it can also be used to estimate the statistical information in simple jet passes by solving deterministic equations. This approach, together with previous investigations developed by Billingham et al. [13] on how to predict the average jet footprint, can readily be extended to larger features generated by multiple jet passes, enabling the use of AWJ milling to manufacture 3D complex parts in high performance materials with reduced variability. To generate such complex parts, it is necessary to find a jet path that will generate the desired shape. Since different strategies, such as random paths or parallel jet passes, can be used to obtain the same average surface, there may be more than one suitable path. However, each jet path will generate parts with different variability, and therefore a method to predict such variations is essential to choose the jet path that will produce optimum results.

2. Stochastic modelling of AWJM

An explanation of the proposed model is presented in this section. A short introduction of how to predict the evolution of the average jet footprint profile is presented first. Then, each of the elements that are proposed to model the fluctuations of the process are explained in detail.

(a) Prediction of the average jet footprint

The main idea of the model presented in [12] can be written as

$$\frac{\partial Z(X,t)}{\partial t} = \Psi(X,Z,t). \tag{2.1}$$

The aim of using such a model is to determine how the surface of the workpiece $Z(X,t)$, evolves when the jet, represented by an etching rate function $\Psi(X,Z,t)$, moves over the surface. To obtain the final jet footprint profile, $Z(X,T)$, (2.1) is solved during the time, T, taken by the jet to complete a full pass over a certain line, usually taken as $Y=0$ for convenience, as is illustrated in figure 3. This approach was extensively validated for multiple experimental parameters and is able to simulate overlapping jet passes and non-normal attack angles. The method was only designed to predict the average evolution of the system, and the limitations of this model are the main motivation of our work.

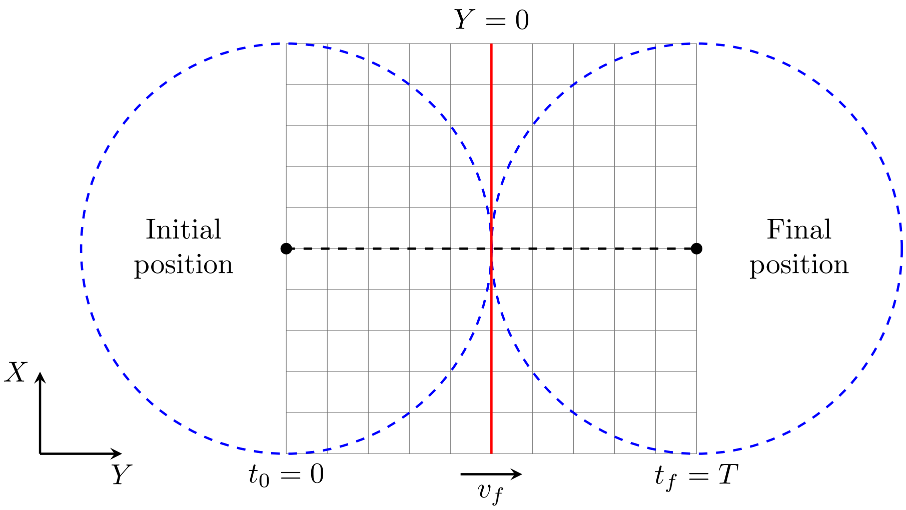

Figure 3: A full jet pass over a given line is required to simulated the average jet footprint profile.

Taking advantage of the symmetry of the problem when modelling single straight jet passes, r is defined as the distance from a given point along $Y=0$ to the centre of the jet at any time t,

$$r^2 = X^2 + (v_f t)^2. \tag{2.2}$$

Equation (2.1) can then be rewritten as

$$\frac{\partial Z(X,t)}{\partial t} = \mu(r) g(Z,t), \tag{2.3}$$

where $\mu(r)$ is the etching rate function and $g(Z,t)$ represents the nonlinear effects of the process. It has been found that for shallow trenches (i.e. large feed speeds), a linear model can be used to predict the average trench profile [21], and therefore the problem can be stated as

$$\frac{\partial Z(X,t)}{\partial t} = \mu(r) \quad \text{for} \quad 0 < t < T. \tag{2.4}$$

As will be shown later, this can be inverted to obtain $\mu(r)$ by using experimental data from milled trenches performed at high feed speeds, $Z(X,T)$.

(b) Stochastic model

In order to cope with the variability of the process, a new framework, based on modelling the system using a stochastic partial differential equation is proposed. The proposed equation must be capable of accounting for different sources of fluctuations, such as the randomness of the particles within the jet and the variability of the pressure in the pump that leads to variations of the mass flow and velocities of the particles. In its most general form, this equation is

$$dZ = \mu(\boldsymbol{X}, Z, t)dt + f(\boldsymbol{X}, Z, t)\left[dW(\boldsymbol{X}, t) + d\xi(t)\right], \tag{2.5}$$

where $\boldsymbol{X} = (X, Y)$, $\mu(\boldsymbol{X}, Z, t)$ is the deterministic erosion rate function, $dW(\boldsymbol{X}, t)$ represents an isotropic Gaussian random field with a given covariance structure (C) [22], $d\xi(t)$ is an Ornstein-Uhlenbeck process [23], and f accounts for the radial dependence of the variability. Therefore, the equation has two stochastic components, $dW(\boldsymbol{X}, t)$ and $d\xi(t)$, that model the noise during the process. Since the solution of (2.5) at a given time T is not deterministic, one can only study either single realisations or the statistical moments of the solution. The model has a deterministic and a stochastic part that play different roles. On the one hand, the deterministic etching rate accounts for the average erosion power of the jet. On the other hand, the stochastic terms contain information regarding the varying part of the system, and can be used to model the properties of such variations. The advantages of this stochastic modelling approach are two-fold: (i) it is a more realistic modelling framework to investigate a system with uncertainties and fluctuations; (ii) it makes it possible to estimate the bounds of such fluctuations and thereby determine the expected quality of the machined features, providing a new tool for further research to minimise these deviations without performing extensive experimental tests. Each term of (2.5) will be described in detail in the following sections.

(i) Definition of the random field

The second term on the right-hand side of (2.5) is a Gaussian isotropic random field [22], $dW(\boldsymbol{X}, t)$, whose variables follow a standard normal distribution. The role of this term is to model the randomness of the particles within the jet, since it is known that their position within the jet, velocity, size and shape are random and this variability is transferred to the milled surface [19]. It is considered reasonable to use a Gaussian field to simulate the variability, although other options could be considered if there was information about the system that suggested otherwise. The field is stationary, so the mean is independent of the position within the jet, and the correlation between two points depends only on the distance between them. This correlation structure is used because the size of the abrasive particles, which are considered to be the main erosion entities, is comparable to the jet size [24]. The particles cannot therefore be considered as point masses, and the length-scale of the noise takes this issue into account. One of the assumptions of this model is that the random fields are not correlated in time, since the particles hit the surface independently in time. Furthermore, it is considered isotropic owing to the symmetry of the problem.

Conceptually, these properties imply that the random values of points that are close to each other are not independent. Mathematically, this field can be decomposed using the eigenvalues and eigenfunctions of the correlation kernel, as stated by the Karhunen-Loève theorem [25]. The field $dW(\boldsymbol{X}, t)$ has a spectral decomposition:

$$dW(\boldsymbol{X}, t) = \sum_{n=1}^{\infty} \sqrt{\lambda_n} \varphi_n(\boldsymbol{X}, t) d\zeta_n(t), \tag{2.6}$$

where λ_n and ϕ_n are the eigenvalues and eigenfunctions of the correlation kernel of the Gaussian random field, and $d\zeta_n(t)$ are independent Wiener processes. An example of a realisation of a random, field with such characteristics is shown in figure 4a. It must be noted that the sum in (2.6) is truncated in order to compute a realisation of a given random field.

(ii) Mean-reverting stochastic process

Although the randomness of the particles plays a significant role in the variability of the milled trench, it is not the only feature of AWJ milling responsible for the large fluctuations observed in the milled surfaces. By modelling only these uncertainties, it was found in [19] that the noise is underestimated compared to experimental data. The approach presented here aims to be more general, providing mechanisms to account for different sources of fluctuations. For this purpose, an Ornstein-Uhlenbeck process is introduced to account for the variability caused by the random variations of the system, such as changes in the pressure or instabilities in the entrainment process. The term $d\xi(t)$ in (2.5) accounts for this process, and is given by

$$d\xi(t) = \theta(\nu - \xi(t))dt + \sigma d\eta(t). \tag{2.7}$$

This is a mean-reverting stochastic process where θ, ν and σ are model parameters and $d\eta$ is a Wiener process. An example of a realisation of an Ornstein-Uhlenbeck process is shown in figure 4b.

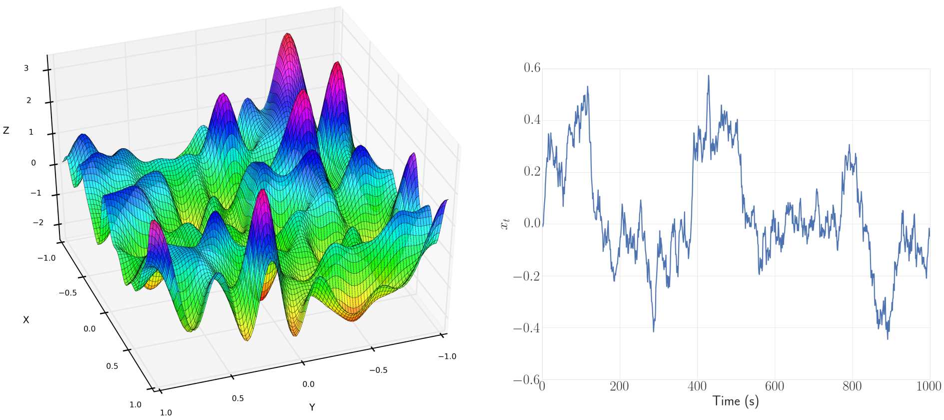

(a) (b)

Figure 4: Stochastic structures used to model the variability during AWJM controlled-depth milling. a) Realisation of a Gaussian random field with an exponential correlation kernel. b) Example of an Ornstein-Uhlenbeck process.

(iii) Radial dependence of the variability

The model described in this section can be used to predict the variability across the jet footprint at different jet feed speeds. However, the parameters of the model are unknown for a given set of experimental conditions. Following the ideas developed in [12,13], a framework to estimate such parameters from a small number of experimental tests is provided here. The potential of this method lies in its ability to calibrate these parameters quickly for any material, jet size, equipment and, eventually, other similar processes. A detailed explanation of how to perform such estimations is provided in the following section.

3. Parameter Estimation

We have developed a procedure to estimate the following attributes: i) the deterministic etching rate function, $\mu(r)$; ii) the parameters that affect the standard deviation across the trench, σ, θ, b_1 and b_2; iii) the correlation structure of the Gaussian field, C. For this investigation, the jet feed speed has been restricted to a range where the evolution of the average trench profile has been found to be linear, as in [21]. One can then rewrite (2.5) as

$$dZ = \mu(r,t)dt + f(r,t)\left[dW(\boldsymbol{X},t) + d\xi(t)\right]. \tag{3.1}$$

Using (3.1), the final surface after one jet pass can be predicted by integrating

$$Z(\boldsymbol{X},T) = \int_0^T \{\mu(r,t)dt + f(r,t)\left[dW(\boldsymbol{X},t) + d\xi(t)\right]\}. \tag{3.2}$$

Since the solution of (3.2) is not deterministic, the required information can only be extracted by studying the expectations of this integral. The Itô interpretation has been used throughout this work, since the fluctuations that are modelled correspond to discrete pulses (i.e. particle impacts) that are independent from each other [26], and therefore information about future events is not known at any given moment.

(a) Etching rate function

The etching rate function, $\mu(r)$, determines the mean erosion rate of the jet and can be found by using the average profile of a single trench [11]. It is therefore necessary to show how to recover this method when using a stochastic framework.

Theorem 3.1. *Taking the expected value of the etched surface, represented in (3.2), leads to*

$$\mathbb{E}\left[Z(\boldsymbol{X},T)\right] = \int_0^T \mu(r,t)dt. \tag{3.3}$$

This recovers the calibration procedure from previous work [12], and allows us to obtain the etching rate function $\mu(r)$, since the expectations of the two last terms on the right-hand side of (3.2) are each zero. The proof of theorem 3.1 is given in the Appendix A.

(b) Estimating the variability

The expected value of the surface does not provide information regarding the variability of the process. Taking the covariance makes it possible to estimate the other parameters of the model. Before doing this, remember that

$$\sigma(X,Y) = \mathbb{E}\left[(X-\mathbb{E}[X])(Y-\mathbb{E}[Y])\right] = \mathbb{E}\left[XY\right] - \mathbb{E}\left[X\right]\mathbb{E}\left[Y\right]. \tag{3.4}$$

In this case, these terms would be

$$X = \underbrace{\int_0^T \mu(r,t)dt}_{\text{a}} + \underbrace{\int_0^T f(r,t)d\xi(t)}_{\text{b}} + \underbrace{\int_0^T f(r,t)dW(\boldsymbol{X},t)}_{c}, \tag{3.5}$$

and

$$Y = \underbrace{\int_0^T \mu(r',t)dt}_{\text{a}'} + \underbrace{\int_0^T f(r',t)d\xi(t)}_{\text{b}'} + \underbrace{\int_0^T f(r',t)dW(\boldsymbol{X}',t)}_{c'}. \tag{3.6}$$

In order to compute $\sigma(X,Y)$, it is necessary to study

$$\mathbb{E}\left[XY\right] = \mathbb{E}\left[(a+b+c)(a'+b'+c')\right], \tag{3.7}$$

where the crossed terms are symmetric, such as $\mathbb{E}\left[ab'\right] = \mathbb{E}\left[ba'\right]$. This can be addressed term by term:

(i) $\mathbb{E}\left[aa'\right]$

$$\mathbb{E}\left[aa'\right] = \mathbb{E}\left[X\right]\mathbb{E}\left[Y\right]; \tag{3.8}$$

and this will cancel out with $\mathbb{E}\left[X\right]\mathbb{E}\left[Y\right]$ in (3.4).

(ii) $\mathbb{E}\left[ac'\right]$

$$\mathbb{E}\left[ac'\right] = \mathbb{E}\left[a\right]\mathbb{E}\left[c'\right] + \sigma(a,c') = 0 \tag{3.9}$$

since $\mathbb{E}\left[c'\right] = 0$ and $\sigma(a,c') = 0$. The same reasoning applies to $\mathbb{E}\left[bc'\right]$ and $\mathbb{E}\left[ab'\right]$.

(iii) $\mathbb{E}\left[cc'\right]$

This term, which contains the correlated random field, has to be studied carefully. It is easier to analyse the simple case of a non-correlated field first, and then include the correlation structure.

Theorem 3.2. *If $dW(\boldsymbol{X'})$ is a non-correlated Gaussian random field, then*

$$\begin{aligned}\mathbb{E}\left[cc'\right] &= \mathbb{E}\left[\int_0^T f(r,t)dW(\boldsymbol{X},t)\int_0^T f(r',t)dW(\boldsymbol{X'},t)\right]\\ &= \int_0^T f(r,t)f(r',t)dt\end{aligned} \tag{3.10}$$

The proof of theorem 3.2 is shown in Appendix B. Equation (3.10) is useful because it provides a mechanism to estimate the covariance matrix in this particular case without solving any stochastic integral. However, since an assumption of the model is that the random field has a correlation structure, it is necessary to investigate how (3.10) behaves in this case.

Theorem 3.3. *If $dW(\boldsymbol{X'})$ is a correlated Gaussian random field,*

$$\mathbb{E}\left[cc'\right] = \sum_{n=1}^{\infty}\lambda_n\int_0^T \varphi_n(\boldsymbol{X},t)\varphi_n(\boldsymbol{X'},t)f(\boldsymbol{X},t)f(\boldsymbol{X'},t)dt. \tag{3.11}$$

where φ_n and λ_n are the eigenfunctions and eigenvalues of the Karhunen-Loève expansion shown in (2.6).

The proof of theorem 3.3 is given in Appendix C.

(iv) $\mathbb{E}\left[bb'\right]$

Theorem 3.4. *The expression*

$$\mathbb{E}\left[bb'\right] = \mathbb{E}\left[\int_0^T f(r,t)d\xi(t)\int_0^T f(r',t)d\xi(t)\right], \tag{3.12}$$

where $d\xi(t)$ is an Ornstein-Uhlenbeck process, can be written as

$$\mathbb{E}\left[bb'\right] = \sigma^2 e^{\left(-2\theta\int_0^T f(r,s)ds\right)}\left(\int_0^t e^{\theta\int_0^t f(r,s)ds}e^{\theta\int_0^t f(r',s)ds}f(r,t)f(r',t)dt\right). \tag{3.13}$$

The proof of theorem 3.4 is provided in Appendix D.

Note that $\boldsymbol{X}$ and $\boldsymbol{X'}$ are points along a profile over which the jet has completely passed, such as the red line shown in figure 3. This provides enough information to compute the variance, since all the points along the chosen profile have been affected by a full jet pass; and for the correlation between different points, making it possible to establish the relation between a set of points that have been fully impinged by the jet. Therefore, this mechanism makes it possible to compare the estimated covariance structure from either experimental and simulated data with an estimate obtained by solving a simple deterministic integral. Furthermore, using single profiles to estimate the covariance structure is a significant advantage, since the same data can be used to estimate the etching rate and other statistical parameters of the problem at the same time.

Both functions μ and f are assumed to be functions of r, the distance to the centre of the jet. The equation to be solved in order to estimate the model parameters for the variability is then

$$\begin{aligned}\sigma(Z,Z') &= \mathbb{E}\left[cc'\right] + \mathbb{E}\left[bb'\right]\\ &= \sum_{n=1}^{\infty}\lambda_n\int_0^T \varphi_n(\boldsymbol{X},t)\varphi_n(\boldsymbol{X'},t)f(\boldsymbol{X},t)f(\boldsymbol{X'},t)dt +\\ &\quad \sigma^2 e^{\left(-2\theta\int_0^T f(r,s)ds\right)}\left(\int_0^t e^{\theta\int_0^t f(r,s)ds}e^{\theta\int_0^T f(r',s)ds}f(r,t)f(r',t)dt\right).\end{aligned} \tag{3.14}$$

The function $f(r)$ can be estimated using only the variance

$$
\begin{aligned}
Var(Z) = & \int_0^T f(r,t)^2 dt + \\
& \sigma^2 e^{\left(-2\theta \int_0^T \mu(r,s)ds\right)} \left(\int_0^T e^{2\theta \int_0^t \mu(r,s)ds} \mu(r,t)^2 dt \right).
\end{aligned} \tag{3.15}
$$

Once $f(r)$ is known, the correlation length-scale can be determined making use of the full covariance matrix. Both (3.14) and (3.15) can be computed numerically. The strength of this framework resides in developing a non-stochastic expression for the covariance matrix that accounts for the erosion process, making it possible to use AWJ milled trenches to estimate the process variance, $f(r)$, and use it to generate complex shapes. Note that the expected value and the covariance can be estimated for single straight passes, but more complex features could be investigated approximating (3.2) numerically with the Milstein method [27], and using Monte Carlo methods to study the expectations of the generated surface.

4. Application to abrasive waterjet machining

The explanation of the model has been kept as generic as possible so far in order to provide a consistent framework that could be extended to other problems in energy beam processing [28]. In this section, the model is illustrated for AWJ milling.

(a) Correlation structure of the Gaussian random field

The correlation kernel for the random field is assumed to be Gaussian, since it is expected that points that are further away than the size of the particles will have no correlation. This kernel can be written, for one dimension, as

$$K(x,x') = e^{-\varepsilon^2 (x-x')^2}. \tag{4.1}$$

The eigenvalue problem for this kernel is

$$\int_{-a}^{a} e^{-\varepsilon^2 (x-x')^2} \phi(y) dy = \lambda \phi(x), \tag{4.2}$$

and it can be solved analytically [29]. The eigenvalues are given by

$$\lambda_i = \frac{\alpha \varepsilon^{2n}}{\left(\frac{\alpha^2}{2} \left(1 + \sqrt{\left(1 + \left(\frac{2\varepsilon}{\alpha} \right)^2 \right)} + \varepsilon^2 \right) \right)^{0.5+n}}, \tag{4.3}$$

and the eigenfunctions have the form

$$\phi_i(x) = \frac{\sqrt[8]{1 + \left(\frac{2\varepsilon}{\alpha}\right)^2}}{\sqrt{2^n n!}} e^{-\left(\sqrt{\left(1+\left(\frac{2\varepsilon}{\alpha}\right)^2\right)} - 1 \right) \frac{\alpha^2 x^2}{2}} H_n \left(\sqrt[4]{1 + \left(\frac{2\varepsilon}{\alpha} \right)^2} \alpha x \right) \tag{4.4}$$

with the local length-scale parameter ε, the weigh function $\rho(x) = e^{-\alpha^2 x^2}$ that localizes the eigenfunctions, and the Hermite polynomials H_n. Since the two-dimensional exponential kernel is separable, these 1D results can easily be extended to 2D. The correlation kernel can be written as

$$C(\boldsymbol{X}, \boldsymbol{X}') = e^{-\left(\varepsilon_1^2 (X_1 - X_1')^2 + \varepsilon_2^2 (X_2 - X_2')^2 \right)}, \tag{4.5}$$

and the eigenvalues and eigenvectors from (4.3) and (4.4) can be used to construct the solutions for the multidimensional case,

$$\phi_j(\boldsymbol{X}) = \phi_i^1(X_1) \phi_k^2(X_2) \quad , \quad \lambda_j = \lambda_i^1 \lambda_k^2. \tag{4.6}$$

For this model, it is assumed that $\varepsilon = \varepsilon_1 = \varepsilon_2$. These assumptions result in a problem that depends on the correlation length-scale, ε, while the global parameter α is chosen according to the size of the system.

(b) Radial dependence of the variability

Since the spatial distribution of particles within the jet is known to be Gaussian [5], a similar behaviour is expected for the variability. For this reason, the function $f(r;t)$ has been chosen to be Gaussian,

$$f(r) = b_1 e^{-2b_2(r)^2}, \tag{4.7}$$

where $r = r(\boldsymbol{X};t)$ has been defined in (2.2). Then, replacing (4.6) and (4.7) in (3.14), and using the truncated Karhunen-Loève expansion, one can compute explicit expressions to estimate the variance and the covariance. The estimation procedure is then:

(i) Estimate $Cov(Z(\boldsymbol{X},T), Z(\boldsymbol{X}',T))$ using experimental data.

(ii) Compare these data with the predicted variance, and thereby determine four parameters: b_1 , b_2, θ and σ. This optimization can be performed using a global search method, DIRECT-L [30], followed by a local optimization using COBYLA [31] to improve accuracy. This can be carried out minimising the cost function

$$J_1(b_1, b_2, \theta, \sigma) = ||Var_{exp}(Z) - Var_{sim}(Z)||, \tag{4.8}$$

where $Var_{sim}(Z)$ is given by (3.15).

(iii) Find the correlation length scale, ε^{-1}, that minimises the cost function

$$J_2(\varepsilon^{-1}) = \left|\left|Cov_{exp}(Z,Z') - Cov_{sim}(Z,Z')\right|\right|, \tag{4.9}$$

where $Cov_{sim}(Z,Z')$ is given by (3.14).

Although computing the covariance can be expensive (i.e. around 40 minutes, although this depends strongly on the initial guess), the possibility of computing the variance without taking the correlation into account makes it possible to perform the optimization within a reasonable time, up to 8 times faster than in the full case. With the tools explained in previous section, it is now possible to make use of the model to predict the variability of abrasive waterjet milled footprints.

5. Experimental methodology

The machine used to generate the experimental data for this work is a Microwaterjet 3-axis machine developed by Waterjet AG, which can be used with several cutting systems with nozzle diameters from 0.2 to $0.8mm$. The equipment is designed to perform high accuracy cutting operations ($\leqslant 0.01$ mm), and a positioning accuracy of ± 0.003mm. The chosen system has a jet diameter of $0.5mm$, and is used for this research because of its reduced size compared to conventional AWJ nozzles, which are $0.78mm$ or larger, good repeatability in producing circular jets and stability at low pressure (i.e. $< 200MPa$). These conditions make this equipment ideal to test the mathematical concepts presented here. The pressure of the system is provided by a KMT streamline SL-V100D ultra-high pressure pump, with a pressure range from 70 to $400MPa$.

In order to perform AWJ controlled-depth milling, relatively low pressure to control the erosion power of the jet was used. For this reason, and based on preliminary experimental work, the pressure is set to $138MPa$ throughout this testing programme. The abrasive particles used for this study are BARTON HPX #220.The reliability of the surface measurements is enhanced by measuring the milled features *in-situ*; this significantly reduces the alignment errors that might be introduced by moving the workpiece after milling. The channels are measured using a white light interferometer with a measurement range of $1.1mm$, a spot size of $8\mu m$ and an axial resolution of $25nm$. The experimental setup is shown in figure 5.

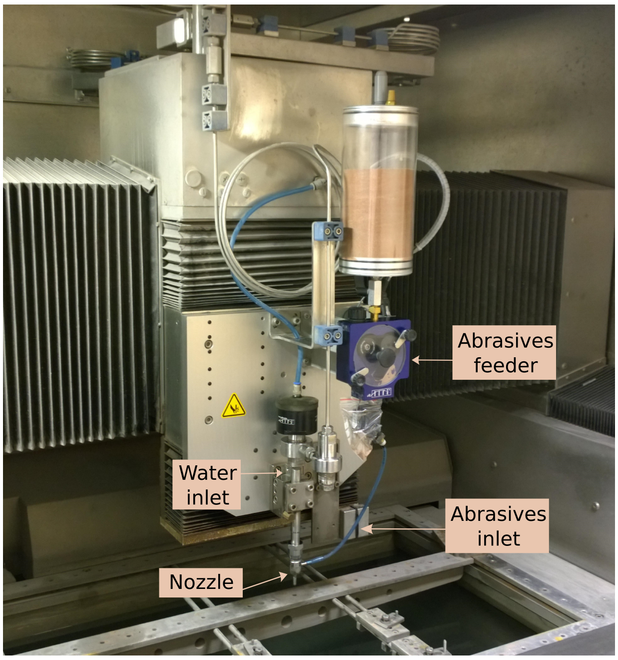

Figure 5: Abrasive microwaterjet machine used to perform experimental tests to validate the model.

P (MPa)	138
$\dot{m}_a (g/s)$	0.5
Nozzle diameter (mm)	0.5
Abrasive mesh size	220
v_f (mm/s)	25.00 - 58.33

Table 1: Operating parameters used to calibrate and validate the model.

The model was validated by performing experimental tests on a Titanium based alloy (Ti-6Al-4V). The objective of the validation step is to show that by performing two sets of jet passes, one at high speed ($58.33mm/s$) and another at low speed ($25mm/s$), it is possible to predict the variability of the jet footprint at any feed speed within this range. The operating parameters used for validation are shown in table 1. In order to gather consistent information on the process, each set of parameters has been repeated 10 times, performing jet passes of $70mm$ length. Figure 6 shows an example of an abrasive waterjet machined trench and an example of the surface data.

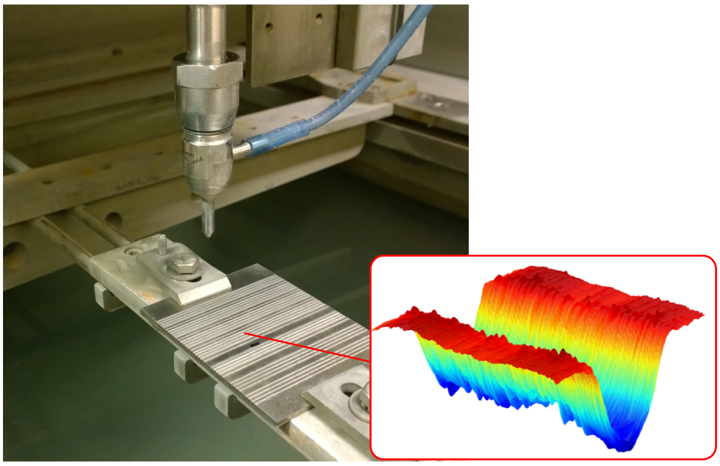

Figure 6: Example of one sample with several jet passes. The surface is scanned to extract 3D data of the abrasive waterjet footprint profiles from experimental data.

The method described in sections 2 and 3 is:

(i) Perform two jet passes at the highest and the lowest feed speeds.
(ii) Use the average profile of the shallow trench to estimate the etching rate function, $\mu(r)$.
(iii) Calibrate the parameters of the variability, b_1; b_2; θ; and σ; using (3.15).
(iv) Using the expression in (3.14), compute the covariance matrix using the data of the shallow trench to estimate the correlation length-scale parameter, ε.
(v) Perform jet passes at different feed speeds within the proposed range to test the predictions performed by the model solving (3.3) for the average profile and (3.15) for the variability.

Note that the last step could also be carried out by performing Monte Carlo simulations solving (3.2) numerically. This approach is computationally more expensive, but it can be used to simulate larger features with complex jet-paths.

6. Results and discussion

The model has been implemented in C++ with extensive use of the linear algebra library Armadillo [32] and the optimization package NLopt [33]. This implementation has been developed to approximate numerically the integrals in (3.14) and (3.15), and therefore compute and minimize the cost functions (4.8) and (4.9) to estimate the parameters of the model. After this, the results for single jet passes can be either estimated using (3.14) and (3.15), or alternatively using Monte Carlo methods to evaluate (3.2). The computation time required to perform a complete test, including calibration and validation of the model is less than 10 minutes with a standard computer. This running time is similar to the one required in [12], and could be improved drastically by investigating alternative methods to estimate the parameters. Hence, the framework developed in this investigation provides a method to predict the jet variability, together with the average footprint profile, without increasing the computation costs. This technique could therefore be implemented in CAD/CAM applications to enable the improvement of the quality of abrasive waterjet milled surfaces.

In order to test the validity of the model, the results have been compared from different perspectives. First, numerical results comparing the predicted and experimental variability of the footprint using the full data set are shown; this includes a comparison of the covariance matrices. Second, the statistical properties of single profiles are compared to determine whether the model is adequate to describe the effect of the erosion process on the surface. Third, a discussion of the effectiveness of the calibration procedure is provided, focusing on how the model depends on the quality of the experimental data, since the prediction of the variability can be affected if anomalous results are used to estimate the parameters of the model. The values of the parameters of the model used is shown in table 2.

$b_1\ (mm/s)$	8.47977
$b_2\ \left(mm^{-2}\right)$	$9.41678 \cdot 10^{-2}$
σ	$8.3552 \cdot 10^{-2}$
θ	$8.3249 \cdot 10^{-2}$
$\varepsilon^{-1}\ (mm)$	0.1241

Table 2: Parameters of the model.

(a) Validation of the model

The results of the model have been tested using 10 sets of milled channels at different feed speeds, as shown in table 1. Figure 7 shows the comparison of the average waterjet footprint profile at different jet feed speeds. The use of a linear model provides a good estimation of the average shape of the footprint, although this may need to be adapted for different materials or more complicated features; previous examples [12,13] show how this may be carried out.

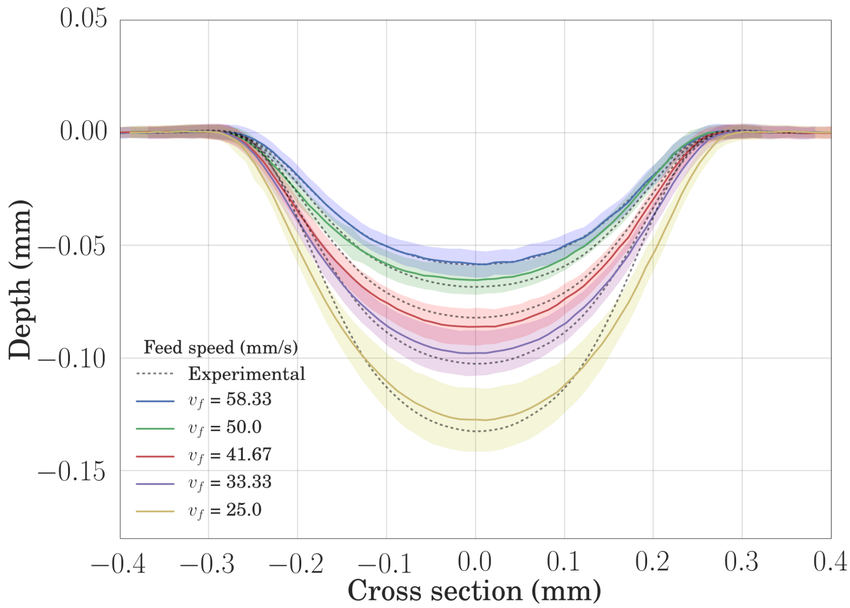

Figure 7: Average kerf profiles at different feed speeds. The shadowed area represents the standard deviation of the experimental trenches.

The profiles of the standard deviation across the jet are shown in figure 8a, suggesting that the fluctuations of the process can be estimated reasonably well. This is a promising result because it implies that the noise can be quantified numerically and, at the same time, the profile of such fluctuations can be predicted in advance. This could be potentially used to design smarter jet-path strategies that take the surface quality into account. It must be noted that the shape of the predicted noise profiles differs from the observed ones near the edges of the trench; this is influenced by the choice of $f(r)$, and, therefore, it can be improved by estimating it numerically or finding more appropriate functions. Figure 8b shows the value of the integral of the profiles shown in figure 8a. This is shown to evaluate how the model performs in order to estimate the total noise of the process for single jet passes. It is observed that the model can predict this pattern successfully within the range of jet feed speeds presented here.

The results shown in this section show that the model successfully captures the dependence of the standard deviation of the jet footprint on the jet feed speed. The prediction is better at higher jet feed speed, and this suggests that there may be non-linear effects below $v_f = 25mm/s$ that affect the noise when the aspect ratio is larger. This is a limitation of the model presented here, and it shows that controlled-depth milling at low jet feed speeds results in large fluctuations, making the process difficult to control and therefore not applicable for industrial manufacturing.

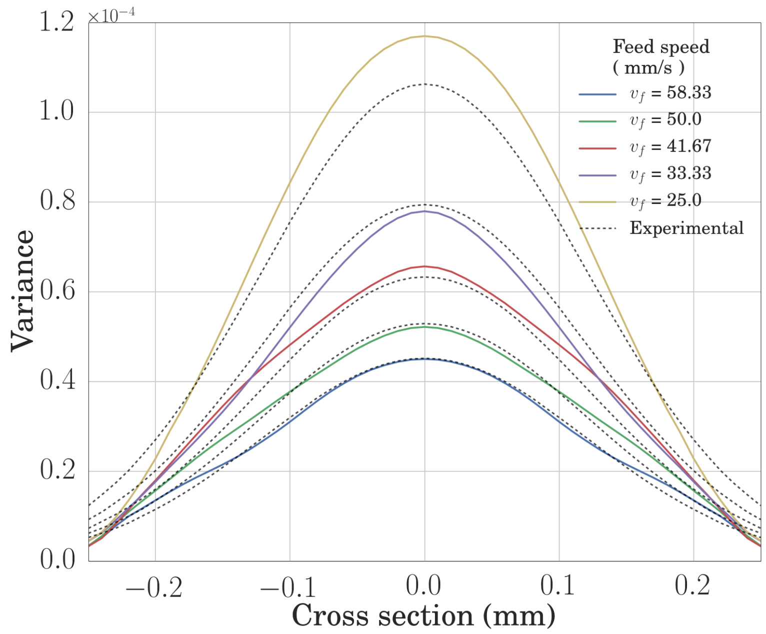

(a)

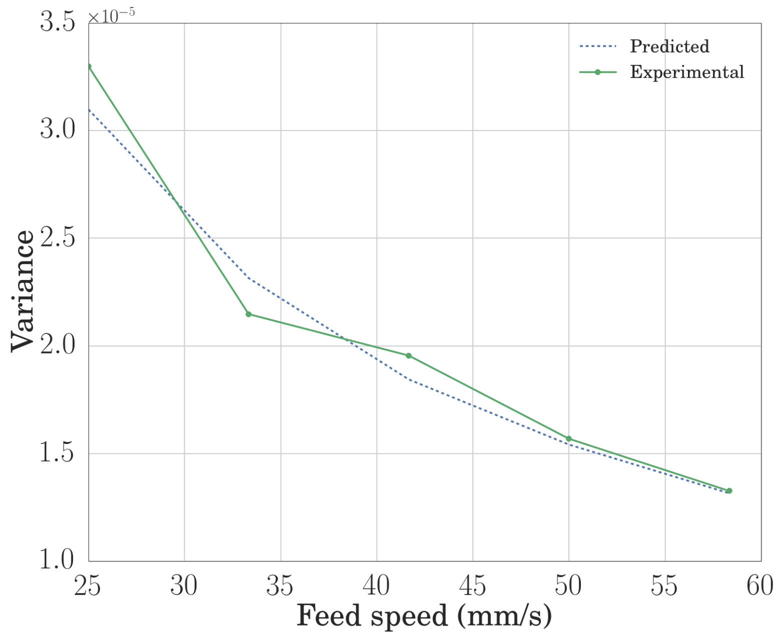

(b)

Figure 8: Comparison of predicted and experimental variance at different jet feed speeds. a) Profile of the variance across the jet footprint. b) Evolution of the uncertainty of the trench profile with the jet feed speed.

(b) Properties of the milled surface

The proposed framework has been proven to be adequate to predict the variability across the jet footprint. Another aspect that the model takes into account is the correlation between different points in the workpiece, as explained in section 2(b)i, since the capability of predicting the statistical properties of the surface is important. Figure 9a shows the estimated covariance matrix from a single experimental jet pass, and this can be compared to the estimated covariance from the simulated case. It is observed that the model successfully captures the correlation between different points within the surface using an exponential correlation kernel. It must be noted that this feature could be changed if the process showed different properties, either by using a different kernel or by estimating the correlation structure from experimental data.

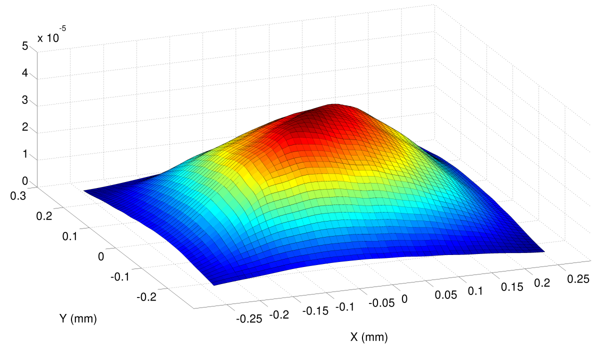

(a)

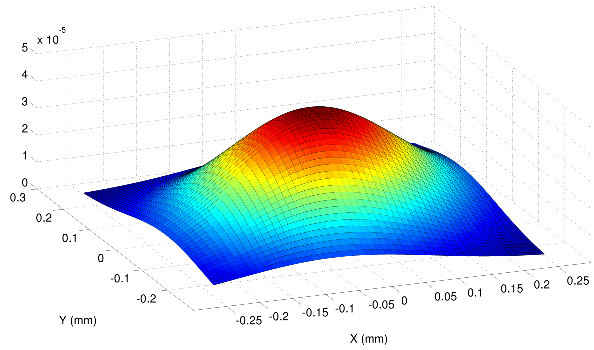

(b)

Figure 9: Comparison of predicted and experimental covariance of abrasive waterjet milled trenches with a jet feed speed $v_f = 58.33mm/s$. a) Experimental covariance matrix. b) Predicted covariance with an exponential correlation kernel.

The introduction of the correlation is a key element of predicting statistical information of the etched surface, and this feature can provide an insight into the suitability of the process for a given application by taking into account such information. However, it must be noted that including this effect has a significant computational cost, and it could be removed if it was not relevant for a particular problem.

(c) Dependence of the method on available data

The proposal of a stochastic model for AWJ milling acknowledges the high variability inherent in the process. The method provided to estimate the parameters of the model relies on the use of good quality data to yield the right set of parameters. However, performing only two jet passes at different speeds does not yield significant information, since single realisations of non-deterministic processes are not meaningful. Figure 10 shows the average results obtained with 10 data sets, as in figure 8b, together with the experimental result of each individual data set. The risk of using a single set of results is clear from the observation of single sets. In figure 10f, the model would underestimate significantly the noise at low speeds, and this would cause an underestimation of the variability for higher jet feed speeds because this result is used for calibration. A different case, in 10g, shows that the variability at $v_f = 50mm/s$ is lower than at $v_f = 58.33mm/s$. Should this jet feed speed interval be the velocity range of interest for a given problem, an anomalous result such as this one would yield a completely opposite outcome from the pattern that is expected of this process and, eventually, would give unsatisfactory results.

The purpose of this comment is to explain the limitations of the model, since dealing with a stochastic system in a manufacturing process implies that the uncertainties may lead to unexpected results in some cases. By using techniques to predict the variability, such as the method presented in this paper, one can develop techniques to minimize this risk. At the same time, it reinforces the idea that quality and amount of data used for calibration is important, and this must be taken into account when implementing a methodology that includes this model.

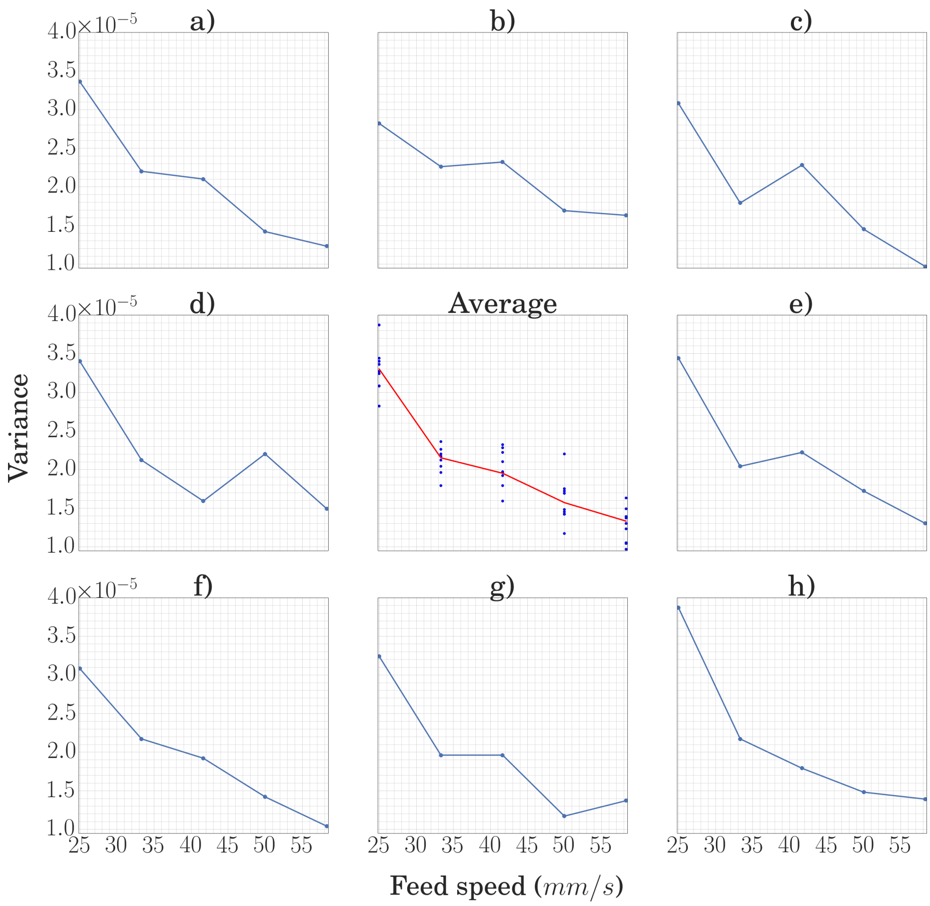

Figure 10: Comparison of the average results with individual data sets.

7. Conclusions

In contrast to conventional methods that aim to predict the mean depth-of-cut or kerf profile, the work presented here proposes a new mathematical framework that is appropriate not only to describe the average outcome of AWJ controlled-depth milling, but also for predicting the variability of an AWJ machined surface for different operating parameters. The model developed in this paper makes it possible to relate theoretical and experimental aspects of the variability of the process and it can be implemented into the most advanced AWJ machines to generate 3D free-forms with the existing technology. By accounting for the stochastic nature of the process, this new approach presents a more realistic model for AWJM since it can be used to enhance the capabilities of current AWJ machines by choosing jet path strategies that minimise the variability. Moreover, since the model is based on a stochastic partial differential equation that represents the evolution of a surface when it is affected by an energy beam, it could be extended to other energy beam processing methods. The main conclusions of this work are:

- Stochastic partial differential equations have been successfully used to reproduce the statistical properties of an AWJ etched surface. This provides a consistent mathematical framework to predict the variability of AWJ milled trenches to within $< 8\%$ error, and gives us a tool to overcome one of the most important limitations on this growing technology.
- The combination of correlated Gaussian random fields with a mean reverting stochastic process makes it possible to model the different sources of fluctuations in the process, such as the randomness of the impact of the abrasive particles and the noise caused by the equipment.
- The development of a new model calibration procedure proves that using the same data required to estimate the etching rate function, one can evaluate the variance and the correlation length-scale of the process. This maximises the amount of information extracted from the experimental data.
- The use of this method not only makes it possible to predict quantitatively the variability of the AWJ milled surfaces for different feed speeds, but also provides a method to generate simulated surfaces with similar statistical properties to the experimental ones.
- This framework is a significant achievement in AWJ machining research, and for other energy beam processes, since its implementation into jet-path generation routines can help improve the surface quality with existing machines. Since it is a simplified approach, it has the advantage of being a fast prediction tool compared with other approaches, such as finite element analysis or artificial intelligence methods. Compared with other deterministic approaches, this framework could potentially be used to complement monitoring methods by including control of the fluctuations of the system, obtaining online information about the deviation from the expected machined surface without surface measurements.

Further research is required to integrate this method into modelling frameworks to simulate overlapping jet passes and, eventually, into optimization routines to find the most suitable jet-paths to enhance the surface quality after the machining process by minimizing the variability of the etched features.

Data accessibility

The data used for this study has been uploaded as electronic supplementary material.

Competing interests

The authors have no competing interests.

Authors' contributions

PLT carried out the development and implementation of the mathematical model, experimental work and drafted the manuscript. JB contributed to the mathematical development of this work and helped draft the manuscript. DA coordinated the project, supported the experimental work and helped draft the manuscript. All authors gave final approval for publication.

Acknowledgements

The authors would like to thank Prof. Michael Tretyakov from the University of Nottingham for his valuable comments and support.

Funding statement

This work has been performed within the EU Initial Training Network STEEP (Grant No. 316560).

Ethics statement

This work did not pose any ethical issues.

rspa.royalsocietypublishing.org Proc R Soc A 0000000

Appendix A.

Proof. To prove that the expected values of the stochastic terms in (3.2) are zero, we can analyze them independently. Since $dW(\boldsymbol{X})$ is a correlated Gaussian random field as discussed in section i, it has a spectral decomposition given by (2.6). The expected value of this term is therefore

$$\begin{aligned}\mathbb{E}\left[\int_0^T f(\boldsymbol{X}_i,t)dW(\boldsymbol{X}_i,t)\right] &= \mathbb{E}\left[\int_0^T \sum_{n=1}^{\infty} \sqrt{\lambda_n}\varphi_n(\boldsymbol{X}_i,t) f(\boldsymbol{X}_i,t) d\zeta_n(t)\right] \\ &= \sum_{n=1}^{\infty} \sqrt{\lambda_n}\varphi_n(\boldsymbol{X}_i,t)\,\mathbb{E}\left[\int_0^T f(\boldsymbol{X}_i,t)d\zeta_n(t)\right],\end{aligned} \tag{A.1}$$

It can be then shown that, if f is bounded,

$$\mathbb{E}\left[\int_0^T f(\boldsymbol{X}_i,t)d\zeta_n(t)\right] = \int_0^T f(\boldsymbol{X}_i,t)\,\mathbb{E}\left[d\zeta_n(t)\right] = 0, \tag{A.2}$$

since $d\zeta_n(t)$ represents a Wiener process, therefore proving that the expectation of the term representing the random field is zero. The same reasoning can be used for the other term, by taking into account that

$$\mathbb{E}\left[d\xi(t)\right] = 0, \tag{A.3}$$

when its mean, ν, and initial value are zero. □

Appendix B.

Proof. Assume that $dW(\boldsymbol{X}',t)$ is uncorrelated noise, and define

$$\varepsilon = \mathbb{E}\left[\int_0^T f(\boldsymbol{X},t)dW(\boldsymbol{X},t)\int_0^T f(\boldsymbol{X}',t)dW(\boldsymbol{X}',t) - \int_0^T f(\boldsymbol{X},t)f(\boldsymbol{X}',t)dt\right]. \tag{B.1}$$

It must be proved that $\varepsilon = 0$ [34]. For this, we rewrite it in its discrete form

$$\begin{aligned}\varepsilon = \mathbb{E}\Bigg[&\sum_k f(\boldsymbol{X},t_{k-1})\Delta W_k \sum_j f(\boldsymbol{X}',t_{j-1})\Delta W_j - \\ &\sum_k f(\boldsymbol{X},t_{k-1})f(\boldsymbol{X}',t_{k-1})\Delta t_k\Bigg]\end{aligned} \tag{B.2}$$

Now decompose the first term on the right-hand side into three terms:

i) $\sum_{k<j} f(\boldsymbol{X},t_{k-1})f(\boldsymbol{X}',t_{j-1})\Delta W_k \Delta W_j$,
ii) $\sum_{k>j} f(\boldsymbol{X},t_{k-1})f(\boldsymbol{X}',t_{j-1})\Delta W_k \Delta W_j$,
iii) $\sum_{k=j} f(\boldsymbol{X},t_{k-1})f(\boldsymbol{X}',t_{k-1})\Delta W_k^2$.

The first term can be rearranged as

$$\mathbb{E}\left[\sum_{k<j} f(\boldsymbol{X},t_{k-1})f(\boldsymbol{X}',t_{j-1})\Delta W_k \Delta W_j\right] = \sum_{k<j} \mathbb{E}\left[f(\boldsymbol{X},t_{k-1})f(\boldsymbol{X}',t_{j-1})\Delta W_k \Delta W_j\right] \tag{B.3}$$

To simplify, we define

$$A = f(\boldsymbol{X},t_{k-1})f(\boldsymbol{X}',t_{j-1})\Delta W_k, \quad B = \Delta W_j. \tag{B.4}$$

The expected value of a product is therefore

$$\mathbb{E}\left[AB\right] = \int\int abp(a,b)dadb, \tag{B.5}$$

where the joint probability distribution, $p(a,b)$, has the form $p(a)p(b)$ if A and B are independent. Since (B.3) has $k < j$, ΔW_k and ΔW_j are independent, while the functions f are not relevant since they are deterministic. As a result, (B.5) can be written as a product of expectations, $\mathbb{E}[A]\,\mathbb{E}[B]$ and, by definition,

$$\mathbb{E}\left[B\right] = \mathbb{E}\left[\Delta W_j\right] = 0. \tag{B.6}$$

The same steps can be followed to prove the same result for the term *ii*. This simplifies (B.2), which becomes

$$\varepsilon = \mathbb{E}\left[\sum_k f(\boldsymbol{X}, t_{k-1})\Delta W_k f(\boldsymbol{X}', t_{k-1})\Delta W_k - \sum_k f(\boldsymbol{X}, t_{k-1}) f(\boldsymbol{X}', t_{k-1})\Delta t_k\right]. \tag{B.7}$$

Taking the deterministic functions out of the expectation gives

$$\varepsilon = \sum_k f(\boldsymbol{X}, t_{k-1}) f(\boldsymbol{X}', t_{k-1})\,\mathbb{E}\left[\Delta W_k^2\right] - \sum_k f(\boldsymbol{X}, t_{k-1}) f(\boldsymbol{X}', t_{k-1})\Delta t_k, \tag{B.8}$$

and finally $\varepsilon = 0$, since $E\left[\Delta W_k^2\right] = \Delta t_k$, proving Theorem 3.2.

□

Appendix C.

Proof. Equation (3.10) can be rewritten using the Karhunen-Loève expansion as

$$\mathbb{E}\left[cc'\right] = E\left[\int_0^T f(\boldsymbol{X}, t) \sum_{n=1}^{\infty} \sqrt{\lambda_n}\varphi_n(\boldsymbol{X}, t) d\zeta_n(t) \int_0^T f(\boldsymbol{X}', t') \sum_{n'=1}^{\infty} \sqrt{\lambda_{n'}}\varphi_{n'}(\boldsymbol{X}', t) d\zeta_{n'}(t)\right]. \tag{C.1}$$

This can be manipulated to get

$$\mathbb{E}\left[cc'\right] = E\left[\int_0^T \int_0^T \sum_{n=0}^{\infty}\sum_{n=0}^{\infty} f(\boldsymbol{X}, t) f(\boldsymbol{X}', t')\sqrt{\lambda_n}\sqrt{\lambda_{n'}}\varphi_n(\boldsymbol{X}, t)\varphi_{n'}(\boldsymbol{X}', t) d\zeta_n(t) d\zeta_{n'}(t)\right], \tag{C.2}$$

and, using the linearity of the expectation,

$$\sigma(Z, Z') = \sum_{n=0}^{\infty}\sum_{n=0}^{\infty} \sqrt{\lambda_n}\sqrt{\lambda_{n'}} E\left[\int_0^T \int_0^T \varphi_n(\boldsymbol{X}, t)\varphi_{n'}(\boldsymbol{X}', t) f(\boldsymbol{X}, t) f(\boldsymbol{X}', t') d\zeta_n(t) d\zeta_{n'}(t)\right]. \tag{C.3}$$

Now, we can obtain equation (3.11) using (3.10) and taking into account that the eigenvectors are orthonormal. □

Appendix D.

Proof. In order to compute this term, we must be able to determine the integral

$$I(T) = \int_0^T f(r,t) d\xi(t). \tag{D.1}$$

This can be done by looking at the solution of a more general stochastic differential equation,

$$dX_t = \{a_1(t)X_t + a_2(t)\} + b_2(t)d\eta(t). \tag{D.2}$$

The solution for this can be obtained using the change of variable

$$d(\ln X_t) = a_1(t)dt, \quad \Phi_{t,t_0} = \exp \int_{t_0}^t a_1(s)ds, \tag{D.3}$$

and applying Itō's lemma to get

$$dY_t = a_2(t)\Phi_{t,t_0}^{-1}dt + b_2(t)\Phi_{t,t_0}^{-1}d\eta(t), \tag{D.4}$$

with

$$U(t,x) = \Phi_{t,t_0}^{-1}x, \quad Y_t = U(t, X_t), \tag{D.5}$$

which has the integral form

$$X_t = \Phi_{t,t_0}\left\{X_{t_0} + \int_{t_0}^t a_2(s)\Phi_{s,t_0}^{-1}ds + \int_{t_0}^t b_2(s)\Phi_{s,t_0}^{-1}d\eta(s)\right\}. \tag{D.6}$$

We take

$$a_1(t) = -\theta f(t) \qquad a_2(t) = 0 \qquad b_2(t) = \sigma f(t), \tag{D.7}$$

and, since $X_{t_0} = 0$,

$$X_t = \sigma\Phi_{t,t_0}\left\{\int_{t_0}^t f(s)\Phi_{s,t_0}^{-1}d\eta(s)\right\}. \tag{D.8}$$

Using (D.8), (3.12) becomes

$$\mathbb{E}\left[bb'\right] = \sigma^2\Phi_{T,0}^2\,\mathbb{E}\left[\int_0^T f(r,s)\Phi_{s,0}^{-1}d\eta(s)\int_0^T f(r',s)\Phi_{s,0}^{-1}d\eta(s)\right]. \tag{D.9}$$

Moreover, replacing

$$\gamma(r,s) = f(r,s)\Phi_{s,0}^{-1}, \tag{D.10}$$

it is easy to see that (D.9) can be rewritten as

$$\mathbb{E}\left[bb'\right] = \sigma^2\Phi_{T,0}^2\,\mathbb{E}\left[\int_0^T \gamma(r,s)d\eta(s)\int_0^T \gamma(r',s)d\eta(s)\right], \tag{D.11}$$

and this expression is similar to (3.10). From this, we can obtain (3.13) by replacing $\gamma(r,s)$ and Φ. □

References

1. D. A. Axinte, B. Karpuschewski, M. C. Kong, A. T. Beaucamp, S. Anwar, D. Miller, and M. Petzel.
High Energy Fluid Jet Machining (HEFJet-Mach): From scientific and technological advances to niche industrial applications.
CIRP Ann.-Manuf. Techn., 63(2):751–771, 2014.
2. A. W. Momber.
Energy transfer during the mixing of air and solid particles into a high-speed waterjet: an impact-force study.
Exp. Therm. Fluid Sci., 25(1-2):31 – 41, 2001.
3. D. K. Shanmugam, J. Wang, and H. Liu.
Minimisation of kerf tapers in abrasive waterjet machining of alumina ceramics using a compensation technique.
Int. J. Mach. Tool Manu., 48:1527–1534, 2008.
4. D.A. Axinte, D.S. Srinivasu, M.C. Kong, and P.W. Butler-Smith.
Abrasive waterjet cutting of polycrystalline diamond: A preliminary investigation.
Int. J. Mach. Tool Manu., 49(10):797–803, August 2009.
5. R. Balz, R. Mokso, C. Narayanan, D. A. Weiss, and K. C. Heiniger.
Ultra-fast X-ray particle velocimetry measurements within an abrasive water jet.
Exp. Fluids, 54(3):1–13, 2013.
6. S. Anwar, D. A. Axinte, and A. A. Becker.
Finite element modelling of abrasive waterjet milled footprints.
J. Mater. Process. Tech., 213:180–193, 2013.
7. M. Takaffoli and M. Papini.
Numerical simulation of solid particle impacts on Al6061-T6 Part II: Materials removal mechanisms for impact of multiple angular particles.
Wear, 296(1-2):648–655, 2012.
8. W. Y. Li, J. Wang, H. Zhu, and C. Huang.
On ultrahigh velocity micro-particle impact on steels: A multiple impact study.
Wear, 309(1):52–64, 2014.
9. J.H.M. ten Thije Boonkkamp and J.K.M. Jansen.
An analytical solution for mechanical etching of glass by powder blasting.
J. Eng. Math., 43(2-4):385–399, 2002.
10. A. Ghobeity, T. Krajac, T. Burzynski, M. Papini, and J. K. Spelt.
Surface evolution models in abrasive jet micromachining.
Wear, 264(3-4):185–198, 2008.
11. D. A. Axinte, D. S. Srinivasu, J. Billingham, and M. Cooper.
Geometrical modelling of abrasive waterjet footprints: A study for 90° jet impact angle.
CIRP Ann.-Manuf. Techn., 59(1):341–346, January 2010.
12. M.C. Kong, S. Anwar, J. Billingham, and D.A. Axinte.
Mathematical modelling of abrasive waterjet footprints for arbitrarily moving jets: Part I - single straight paths.
Int. J. Mach. Tool Manu., 53(1):58–68, February 2012.
13. J. Billingham, C. B. Miron, D. A. Axinte, and M. C. Kong.
Mathematical modelling of abrasive waterjet footprints for arbitrarily moving jets: Part II - Overlapped single and multiple straight paths.
Int. J. Mach. Tool Manu., 68:30–39, May 2013.
14. J.R. Nicholls and D.J. Stephenson.
Monte Carlo modelling of erosion processes.
Wear, 186:64–77, 7 1995.
15. M.A Verspui, G. de With, A. Corbijn, and P.J. Slikkerveer.
Simulation model for the erosion of brittle materials.
Wear, 233–235:436 – 443, 1999.
16. A. Lebar and M. Junkar.
Simulation of abrasive water jet cutting process: Part 1. Unit event approach.
Model. Simul. Mater. Sc., 12(6):1159–1170, November 2004.
17. H. Orbanic and M. Junkar.
Simulation of abrasive water jet cutting process: Part 2. Cellular automata approach.

Model. Simul. Mater. Sc., 12(6):1171–1184, November 2004.

18. Y. Wang and Z. Yang.
Finite element model of erosive wear on ductile and brittle materials.
Wear, 265(5-6):871–878, 2008.
19. P. Lozano Torrubia, D.A. Axinte, and J. Billingham.
Stochastic modelling of abrasive waterjet footprints using finite element analysis.
Int. J. Mach. Tool Manu., 95:39 – 51, 2015.
20. N. Haghbin, J. K. Spelt, and M. Papini.
Abrasive waterjet micro-machining of channels in metals: Comparison between machining in air and submerged in water.
Int. J. Mach. Tool Manu., 88:108–117, January 2015.
21. A. Bilbao Guillerna, D.A. Axinte, and J. Billingham.
The linear inverse problem in energy beam processing with an application to abrasive waterjet machining.
Int. J. Mach. Tool Manu., 99:34 – 42, 2015.
22. G.J. Lord, C.E. Powell, and T. Shardlow.
An Introduction to Computational Stochastic PDEs.
Cambridge Texts in Applied Mathematics. Cambridge University Press, New York, 2014.
23. G. E. Uhlenbeck and L. S. Ornstein.
On the theory of the brownian motion.
Phys. Rev., 36:823–841, Sep 1930.
24. C. Narayanan, R. Balz, D. A. Weiss, and K. C. Heiniger.
Modelling of abrasive particle energy in water jet machining.
J. Mater. Process. Tech., 213(12):2201–2210, December 2013.
25. R. G. Ghanem and P. D. Spanos.
Stochastic finite elements : a spectral approach.
Dover publications, Inc., Mineola, New York, 2003.
26. Peter E Kloeden and Eckhard Platen.
Numerical Solution of Stochastic Differential Equations.
Stochastics An International Journal of Probability and Stochastic Processes, 23:1–7, 1992.
27. G. N. Mil'shtejn.
Approximate integration of stochastic differential equations.
Theor. Probab. Appl +., 19(3):557–562, 1975.
28. D. Gilbert, M. Stoesslein, D. Axinte, P. Butler-Smith, and J. Kell.
A time based method for predicting the workpiece surface micro-topography under pulsed laser ablation.
J. Mater. Process. Tech., 214(12):3077 – 3088, 2014.
29. C. E. Rasmussen and C. K. I. Williams.
Gaussian processes for machine learning., volume 14.
2006.
30. J. M. Gablonsky and C. T. Kelley.
A locally-biased form of the direct algorithm.
J.Global Optim., 21(1):27–37, 2001.
31. M. J.D. Powell.
A direct search optimization method that models the objective and constraint functions by linear interpolation.
In *Advances in optimization and numerical analysis*, pages 51–67. Springer, 1994.
32. C. Sanderson.
Armadillo: an open source C++ linear algebra library for fast prototyping and computationally intensive experiments.
2010.
33. S. G. Johnson.
The NLopt nonlinear-optimization package, 2014.
34. B. Øksendal.
Stochastic differential equations.
Springer Berlin Heidelberg, 2003.